Electron backscattering from surfaces: The invariant-embedding approach

Lev G. Glazov[1] and Sven Tougaard[2,*]
[1]*Institute of High Current Electronics, Akademichesky 4, Tomsk, Russia*
[2]*Physics Department, University of Southern Denmark, DK-5230, Odense M, Denmark*
(Received 15 April 2003; published 10 October 2003)

Distributions of electrons reflected from a solid surface corresponding to a reflection electron energy loss spectroscopy (REELS) experiment are calculated within the invariant-embedding approach. The technique is based upon a formalism recently developed by Vicanek. In this paper we show that the pertinent balance equations readily allow effective numerical evaluation of various electron distributions relevant for REELS. The solutions are very accurate (with the relative errors readily reduced to $\lesssim 10^{-4}$ for given cross sections) and the resulting technique offers significant advantages over the Monte Carlo approach, though it is less generally applicable. The approach delivers, in a single calculation, the probability distributions resolved in the number of elastic as well as inelastic collisions for all angles of incidence and emission. From these results, one readily obtains other related distributions, e.g., path length and energy spectra. Compared to Monte Carlo simulations, the scheme is faster by up to several orders of magnitude while producing a better accuracy. For a wide range of energies and targets, various distributions of backscattered electrons are exemplified and discussed. The elastic-peak results and a procedure for extraction of the inelastic mean free path are tested by comparison to recent Monte Carlo simulations and typically excellent agreement is found; discrepancies observed in a few cases are shown to be due to deficiencies in the Monte Carlo scheme.

DOI: 10.1103/PhysRevB.68.155409 PACS number(s): 68.49.Jk, 79.20.−m, 79.60.−i

I. INTRODUCTION

When a solid surface is bombarded with a monoenergetic beam of electrons, some of these are emitted after having suffered a number of elastic and inelastic collisions. The energy spectrum of backscattered electrons contains valuable information on the electronic excitations in the solid, giving rise to the technique long known as reflection electron energy loss spectroscopy (REELS).[1] Some years ago, a simple algorithm was developed for the determination of the inelastic electron scattering cross section from analysis of an experimental REELS spectrum.[2–4] This method allows quantitative interpretation and has been applied to many solids.[5]

In principle, it is always possible to determine electron fluxes relevant for quantitative analysis of REELS spectra by Monte Carlo simulations cf., for example, Refs. 6–8. However, achieving good statistics in adequate simulations requires typically a very large computational effort, as the calculated fluxes should be ideally resolved in both emission direction and, e.g., the number of collisions or path length. In most applications of REELS, this has resulted in either applying rather rough approximations for the effects of elastic electron scattering or leaving unresolved some of the desired variables.

A similar and related problem arises in connection with the determination of the inelastic electron mean free path (IMFP) from a REELS experiment. This method relies on the fact that the intensity of the *elastically* backscattered electrons depends strongly on the IMFP, which allows one to determine the latter by measuring the former[8–11] and comparing the measurement to model calculations. In this so-called elastic peak electron spectroscopy (EPES) method, the elastic-peak intensity is usually calculated by Monte Carlo simulations of electron trajectories and accurate elastic-scattering cross sections are assumed known, while the IMFP is treated as an adjustable parameter. Although the Monte Carlo calculations are faster when only the elastic peak intensity is needed rather than the distribution of collisions or the full energy spectra, it is still a very time-consuming method. Therefore, various approximate solutions to calculate the elastic peak intensity have been proposed. These include, e.g., the transport approximation[12,13] and expansion in multiple-scattering contributions.[14] Both approximations take advantage of the strong predominance for elastic scattering in the forward direction. In a recent paper[15] the range of validity of some of these models was studied by comparison to Monte Carlo simulations.

Significant progress was recently achieved by Vicanek[6] within the framework of the invariant-embedding approach.[16,17] Vicanek's treatment is based upon balance equations for the distributions of the number of elastic collisions and path lengths for electrons emitted in a given solid angle, which allowed him to establish a simple analytical relation between the two distributions. Finally, the elastic-peak intensity and the inelastic-collision number distribution (of primary interest for EPES and REELS, respectively) are readily determined from the path length distribution, provided that the mean free path for inelastic electron scattering is known.

Although Vicanek's analysis gave invaluable new insight into the fundamental physics of REELS, the numerical calculation technique developed in his paper[6] still relied on Monte Carlo results for one of the distributions. Vicanek then used his analytical relations to calculate the path length, inelastic-collision number, and energy distributions of the emitted electrons from the simulated elastic-collision number distribution. This calculation scheme offers certain advantages[6] but, being ultimately based upon Monte Carlo (MC) results, it still has the corresponding limitations with respect to accuracy and computing time.

In the present paper, though basically following up on Ref. 6, we show that the invariant-embedding equations allow direct calculation of electron fluxes relevant for REELS and EPES. This approach involves no simulations at any stage and, in our opinion, is a powerful alternative to MC-based techniques though is not as generally applicable. It has significant advantages compared to the latter as regards both *accuracy* and *computing speed*. Depending on the set of resolved variables, the technique is faster than comparable Monte Carlo simulations by up to several orders of magnitude. It delivers practically exact results for a given elastic-scattering cross section, and therefore the technique has no difficulty in handling, e.g., cross sections with several maxima and minima in the angular distribution which can cause problems in Monte Carlo simulations.[15] Comparison of the present results to those of recent simulations shows that occassional deviations observed are due to limitations of the Monte Carlo scheme.

Section II below serves to list the basic invariant-embedding equations and the main relations between various distributions of interest; it also considers important general properties of the solutions. In Sec. III, we discuss briefly a numerical technique used to calculate electron fluxes and estimate computing time required. The capabilities of the approach are illustrated in Sec. IV where various exemplary results are presented, discussed, and compared to recent Monte Carlo simulations. Finally, Sec. V briefly considers the main limitations of the approach at present and desirable extensions.

II. INVARIANT-EMBEDDING EQUATIONS AND THEIR PROPERTIES

A. Basic relations

In this subsection we summarize the relevant results by Vicanek,[6] with minor changes of notation and appropriate comments. Although more general treatments should be possible, we will follow Ref. 6 and assume that the medium is semi-infinite and homogeneous, and that the energy variation of all pertinent cross sections as well as angular deflections in the *inelastic* scattering events are negligible. These are reasonable approximations when only the part of the energy spectrum that corresponds to small *relative* energy loss is considered. Though with obvious reservations, the assumptions are usually well fulfilled for calculations relevant for EPES and REELS, which typically use electrons of energy $\geqslant 100$ eV emitted after none or a few inelastic collisions.

Let the solid surface be bombarded by electrons of energy E_0 (parametric dependence on which is omitted in further formulas) and direction of incidence $\mathbf{\Omega}_0=(\theta_0,\phi_0)$; some of these will escape in the direction $\mathbf{\Omega}=(\theta,\phi)$. Here θ_0 and θ denote the incidence and emission angles with respect to the inward surface normal ($0\leqslant\theta_0<\pi/2<\theta\leqslant\pi$; see Fig. 1). Let further $\mathcal{W}_n(\mathbf{\Omega}_0,\mathbf{\Omega})$ be the elastic-collision number distribution; i.e., $\mathcal{W}_n(\mathbf{\Omega}_0,\mathbf{\Omega})d^2\mathbf{\Omega}$ is the probability for an electron incident in direction $\mathbf{\Omega}_0$ to be emitted into the solid angle $(\mathbf{\Omega},d^2\mathbf{\Omega})$ after n elastic collisions.

The basic idea in the invariant-embedding argument is that the distribution of backscattered electrons from a semi-infinite medium is unchanged when a layer (of the same material) is added to the surface. The collisions that take place in the added infinitesimal layer may be divided into four distinct collision processes, the joint effect of which on $\mathcal{W}_n$ must cancel. This leads to the following recurrence relations for $\mathcal{W}_n$ (Ref. 6):

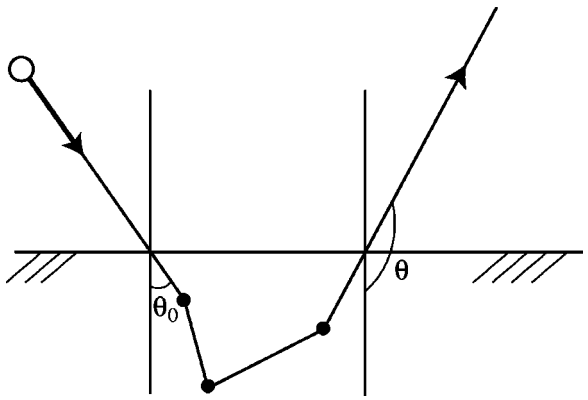

FIG. 1. Schematics of the REELS process considered in the paper. Note that the angles of incidence θ_0 and emission θ are both defined with respect to the inward surface normal.

$$\left(\frac{1}{\cos\theta_0}+\frac{1}{|\cos\theta|}\right)\frac{\mathcal{W}_n}{\lambda_{\rm el}}=\delta_{n1}\mathcal{J}+\mathcal{J}\times\mathcal{W}_{n-1}+\mathcal{W}_{n-1}\times\mathcal{J}+\sum_m \mathcal{W}_m\times\mathcal{J}\times\mathcal{W}_{n-1-m}. \quad (1)$$

Here, $\delta_{n1}=1$ for $n=1$ and $=0$ otherwise, $\lambda_{\rm el}=[N\int\sigma_{\rm el}(\mathbf{\Omega}_0,\mathbf{\Omega})d^2\mathbf{\Omega}]^{-1}$ is the mean free path between elastic collisions, $\mathcal{W}_n=\mathcal{W}_n(\mathbf{\Omega}_0,\mathbf{\Omega})$, $\mathcal{J}=\mathcal{J}(\mathbf{\Omega}_0,\mathbf{\Omega})\equiv N\sigma_{\rm el}(\mathbf{\Omega}_0,\mathbf{\Omega})/|\cos\theta_0|$, N the atomic density of the solid, and $\sigma_{\rm el}(\mathbf{\Omega}_0,\mathbf{\Omega})d^2\mathbf{\Omega}$ the elastic-collision differential cross section for $\mathbf{\Omega}_0\rightarrow\mathbf{\Omega}$ scattering. The symbol $\times$ in Eq. (1) signifies an integration of the type

$$A\times B\equiv\int d^2\mathbf{\Omega}'A(\mathbf{\Omega}_0,\mathbf{\Omega}')B(\mathbf{\Omega}',\mathbf{\Omega}), \quad (2)$$

where the integration interval in each term corresponds to putting $\mathcal{W}_n(\mathbf{\Omega}_0,\mathbf{\Omega})=0$ for $\cos\theta_0<0$ and/or $\cos\theta>0$. For backscattered electrons we may also put $\mathcal{W}_n\equiv 0$ for $n\leqslant 0$, and thus the rightmost term in Eq. (1) vanishes for $n\leqslant 2$ and otherwise the summation extends over the interval $1\leqslant m\leqslant n-2$. The right-hand side of Eq. (1) involves only functions $\mathcal{W}_m$ with $m<n$; i.e., Eq. (1) is in fact an explicit recurrence formula that in principle allows one to evaluate the functions W_n sequentially, starting from the obvious analytical result for $n=1$:

$$\mathcal{W}_1(\mathbf{\Omega}_0,\mathbf{\Omega})=\frac{N\lambda_{\rm el}\sigma_{\rm el}(\mathbf{\Omega}_0,\mathbf{\Omega})|\cos\theta|}{\cos\theta_0+|\cos\theta|}. \quad (3)$$

As shown by Vicanek,[6] the set $\mathcal{W}_n$ at given incidence and emission directions $\mathbf{\Omega}_0,\mathbf{\Omega}$ (or a range thereof) uniquely determines the associated path length and inelastic-collision number distributions $\mathcal{Q}$ and $\mathcal{V}_m$, which are defined as fol-

lows: $\mathcal{Q}(\mathbf{\Omega}_0,\mathbf{\Omega};R)d^2\mathbf{\Omega}\,dR$ and $\mathcal{V}_m(\mathbf{\Omega}_0,\mathbf{\Omega})d^2\mathbf{\Omega}$ are probabilities for an electron incident in the direction $\mathbf{\Omega}_0$ to be emitted into the solid angle $(\mathbf{\Omega},d^2\mathbf{\Omega})$ after having, respectively, traveled the path length (R,dR) and experienced m *inelastic* collisions within the solid. The principle of invariant embedding readily leads to a balance equation for $\mathcal{Q}$ analogous to Eq. (1) (Ref. 6); comparison of the two equations allows one to explicitly relate their solutions:

$$\mathcal{Q}(\mathbf{\Omega}_0,\mathbf{\Omega};R)=\frac{1}{\lambda_{\mathrm{el}}}e^{-R/\lambda_{\mathrm{el}}}\sum_{n=1}^{\infty}\frac{(R/\lambda_{\mathrm{el}})^{n-1}}{(n-1)!}\mathcal{W}_n(\mathbf{\Omega}_0,\mathbf{\Omega}). \tag{4}$$

From the path length distribution, an expression for the inelastic-collision number distribution $\mathcal{V}_m(\mathbf{\Omega}_0,\mathbf{\Omega})(m=0,1,\ldots)$ is found by applying Poisson statistics for each path length:[6]

$$\mathcal{V}_m(\mathbf{\Omega}_0,\mathbf{\Omega})=\frac{1}{m!}\int_0^{\infty}\mathcal{Q}(\mathbf{\Omega}_0,\mathbf{\Omega};R)\left(\frac{R}{\lambda_{\mathrm{in}}}\right)^m e^{-R/\lambda_{\mathrm{in}}}\,dR \tag{5}$$

$$=\sum_{n=1}^{\infty}\frac{(n+m-1)!}{m!(n-1)!}\frac{\lambda_{\mathrm{el}}^m\lambda_{\mathrm{in}}^n}{(\lambda_{\mathrm{el}}+\lambda_{\mathrm{in}})^{m+n}}\mathcal{W}_n(\mathbf{\Omega}_0,\mathbf{\Omega}), \tag{6}$$

where λ_{in} is the inelastic mean free path. Finally, the energy loss distribution is readily determined as (elastic peak excluded)

$$F_1(\mathbf{\Omega}_0,\mathbf{\Omega},T)=\sum_{m=1}^{\infty}\mathcal{V}_m(\mathbf{\Omega}_0,\mathbf{\Omega})\kappa_m(T), \tag{7}$$

where κ_m is the m-fold convolution of the normalized excitation cross section $\kappa(T)$ (Ref. 6):

$$\kappa_m(T)=\int\kappa_{m-1}(T')\kappa(T-T')dT'. \tag{8}$$

In Eqs. (4)–(8) the quantities of interest are expressed in terms of the elastic-collision number distribution. The determination of the latter is then the only nontrivial task for evaluation of quantities pertaining to electron backscattering from solids. Thus, with $\mathcal{W}_n$ and relevant mean free paths given, one immediately obtains $\mathcal{Q}$ and $\mathcal{V}_m$ by means of Eqs. (4)–(6). On the other hand, Eq. (6) with $m=0$ is the elastic-peak intensity. This can be used to determine λ_{in}, as commonly done for EPES, by adjusting λ_{in} until $\mathcal{V}_0$ equals the measured elastic-peak intensity. Having calculated $\mathcal{V}_m$, one may further evaluate the REELS energy spectrum from Eq. (7) utilizing available energy loss cross sections, e.g., the approximate ''universal'' cross sections.[18] Alternatively, from $\mathcal{V}_m$ and a measured REELS spectrum one may determine $\kappa(T)$ applying one of the available simple deconvolution techniques[6,19] to Eqs. (7) and (8).

In Ref. 6, Eq. (1) was utilized for analysis and derivation of Eq. (4) but not for direct calculation of $\mathcal{W}_n$. Instead, in explicit examples, the elastic-collision number distribution was determined by Monte Carlo simulations, while $\mathcal{Q}$, $\mathcal{V}_m$, and F_1 were thereafter calculated from Eqs. (4), (6), and (7). Due to the smoothing effect of the latter formulas, the procedure has the advantage that statistical noise in the determined distributions is reduced considerably compared to what one obtains by their direct Monte Carlo simulation. However, below we demonstrate the inefficiency of this procedure compared to direct calculation of $\mathcal{W}_n$ from the deterministic relations in Eq. (1).

B. Azimuth-integrated distributions

Numerical evaluation of Eq. (1) is of course simpler for the emission intensity integrated over the azimuthal variable ϕ. In order to make the approach more transparent, the present paper limits explicit calculations to azimuth-integrated quantities, and thus graphical examples will refer to the case of normal incidence. Note, however, that calculations with fully resolved azimuths can be performed by the same method, with only minor modifications and *insignificant increase in computing effort*; this will be shown in our forthcoming publication.

For the present calculations, we introduce the azimuth-integrated distributions

$$\begin{Bmatrix} W_n(\eta_0,\eta) \\ Q(\eta_0,\eta;R) \\ V_n(\eta_0,\eta) \end{Bmatrix} \equiv \int_0^{2\pi}\begin{Bmatrix} \mathcal{W}_n(\mathbf{\Omega}_0,\mathbf{\Omega}) \\ \mathcal{Q}(\mathbf{\Omega}_0,\mathbf{\Omega};R) \\ \mathcal{V}_n(\mathbf{\Omega}_0,\mathbf{\Omega}) \end{Bmatrix} d\phi, \tag{9}$$

where $\eta_0\equiv\cos\theta_0$ and $\eta\equiv|\cos\theta|$ are cosines of incidence and emission angles with respect to the inward and outward surface normals, respectively; $0<\eta_0,\eta\leqslant 1$. The physical meaning of the functions in Eq. (9) is rather evident; e.g., $W_n(\eta_0,\eta)d\eta$ is the probability for an electron incident in direction η_0 to be emitted within the cosine interval $(\eta,d\eta)$ after having experienced n elastic collisions. The corresponding distribution in emission *angle* is $W_n(\eta_0,|\cos\theta|)\sin\theta\,d\theta$. Similar interpretations hold for the path-length (Q) and inelastic-collision number (V_m) distributions (see Table I). Implying axial symmetry for elastic scattering, we may express the normalized cross section for elastic collisions as a function of the cosine of the scattering angle:

$$\mathcal{K}(\mathbf{\Omega}_0\cdot\mathbf{\Omega})\equiv\lambda_{\mathrm{el}}N\sigma_{\mathrm{el}}(\mathbf{\Omega}_0,\mathbf{\Omega}),\quad 2\pi\int_{-1}^{1}\mathcal{K}(\eta)d\eta=1. \tag{10}$$

Now by integration of Eq. (1) over azimuths we get the following recurrence formulas for W_n:

$$\left(\frac{1}{\eta_0}+\frac{1}{\eta}\right)W_n=\delta_{n1}J^-+J^+\times W_{n-1}+W_{n-1}\times J^+ + \sum_m W_m\times J^-\times W_{n-1-m}, \tag{11}$$

where $W_n=W_n(\eta_0,\eta)$, the symbol $\times$ denotes now the integration

$$A\times B\equiv\int_0^1 A(\eta_0,\eta')B(\eta',\eta)d\eta', \tag{12}$$

and the kernels $J^{\pm}$ are defined by

TABLE I. Overview of the distribution functions used in the paper. $\eta_0 = \cos\theta_0$ and $\eta = |\cos\theta|$ where θ_0 and θ are the electron incidence and emission angles defined in Fig. 1.

	Probability for an electron incident in direction η_0 to be emitted within the cosine interval $(\eta, d\eta)$ after
$W_n(\eta_0,\eta)d\eta$	having experienced n elastic collisions
$V_{mn}(\eta_0,\eta)d\eta$	having experienced m inelastic and n elastic collisions
$V_m(\eta_0,\eta)d\eta$	having experienced m inelastic collisions
$Q(\eta_0,\eta;R)d\eta\, dR$	having traveled the path length (R, dR) in the solid

$$J^{\pm} = J^{\pm}(\eta_0,\eta) \equiv \frac{1}{\eta_0} K^{\pm}(\eta_0,\eta),$$

$$K^{\pm}(\eta_0,\eta) \equiv \int_0^{2\pi} \mathcal{K}(\pm\eta_0\eta + \sqrt{1-\eta_0^2}\sqrt{1-\eta^2}\cos\phi)\, d\phi. \tag{13}$$

The latter kernels govern transformations of direction cosines *in a single elastic collision*. Thus, for $0 < \eta_0, \eta \leqslant 1$, an electron moving in direction η_0 is scattered into the interval $(\pm\eta, d\eta)$ with the probability $K^{\pm}(\eta_0,\eta)d\eta$. In accordance with this result, for any η_0, $K^{\pm}$ satisfy the normalization condition

$$\int_0^1 [K^+(\eta_0,\eta) + K^-(\eta_0,\eta)]\, d\eta \equiv 1. \tag{14}$$

For a given elastic-collision cross section, formula (11) allows one to recurrently calculate the functions W_n starting from

$$W_n \equiv 0, \quad n \leqslant 0,$$

$$W_1(\eta_0,\eta) = J^-(\eta_0,\eta)\frac{\eta_0\eta}{\eta_0+\eta} = K^-(\eta_0,\eta)\frac{\eta}{\eta_0+\eta}. \tag{15}$$

With minor changes, Eqs. (4)–(7) obviously hold also for the azimuth-integrated functions. The respective formulas for the path-length and inelastic-collision number distributions which will be utilized below, are

$$Q(\eta_0,\eta;R) = \frac{1}{\lambda_{\rm el}} e^{-R/\lambda_{\rm el}} \sum_{n=1}^{\infty} \frac{(R/\lambda_{\rm el})^{n-1}}{(n-1)!} W_n(\eta_0,\eta), \tag{16}$$

$$V_m(\eta_0,\eta) \equiv \sum_{n=1}^{\infty} V_{mn}(\eta_0,\eta), \tag{17}$$

with

$$V_{mn}(\eta_0,\eta) = \frac{(n+m-1)!}{m!(n-1)!} \frac{\lambda_{\rm el}^m \lambda_{\rm in}^n}{(\lambda_{\rm el}+\lambda_{\rm in})^{m+n}} W_n(\eta_0,\eta). \tag{18}$$

Note that the terms V_{mn} defined in Eq. (18) deliver an even more detailed description of the electron fluxes and represent the ''joint'' collision number distribution. Thus $V_{mn}(\eta_0,\eta)d\eta$ is the probability for an electron incident in direction η_0 to be emitted in the direction $(\eta, d\eta)$ after m $(\geqslant 0)$ inelastic and $n(\geqslant 1)$ elastic collisions. Table I gives an overview of the probability distributions considered in the paper.

C. Properties of solutions

Before we make explicit calculations, we consider first some general invariance properties of the distributions defined above. First we note an important symmetry with respect to exchange of incidence and emission directions. Using the obvious property $K^{\pm}(\eta_0,\eta) = K^{\pm}(\eta,\eta_0)$, one easily proves by induction that the functions $W_n(\eta_0,\eta)/\eta$, as determined by Eqs. (11) and (15), are symmetric with respect to the substitution $\eta_0 \leftrightarrow \eta$. From Eqs. (16)–(18), the same result follows for $V_m(\eta_0,\eta)/\eta$ and $Q(\eta_0,\eta,R)/\eta$, i.e.,

$$\eta_0 W_n(\eta_0,\eta) = \eta W_n(\eta,\eta_0),$$

$$\eta_0 Q(\eta_0,\eta;R) = \eta Q(\eta,\eta_0;R),$$

$$\eta_0 V_m(\eta_0,\eta) = \eta V_m(\eta,\eta_0). \tag{19}$$

Another important property of the distributions is implicit in the utilized elastic-collision expansion and the underlying use of the elastic mean free path as the auxiliary model parameter. Typically, the cross sections for elastic scattering are strongly peaked in the forward direction and the detailed cross section for small-angle scattering is very dependent on the particular electron-atom interaction potential used to calculate the cross section.[20] Therefore, as has been pointed out before,[21] the elastic-scattering cross section and the corresponding $\lambda_{\rm el}$ are not well defined. Furthermore, small-angle scattering events have only a weak influence on the electron trajectories and should therefore have negligible effect on measurable physical quantities. For these reasons, it could be argued that expansion in the number of elastic-scattering events might not be a good and efficient choice.

For example, the electron trajectories will be unchanged if we introduce ''collisions'' with negligible angular scattering and transform the cross section from $\sigma_{\rm el}(\mathbf{\Omega}_0,\mathbf{\Omega})$ to

$$\tilde{\sigma}_{\rm el}(\mathbf{\Omega}_0,\mathbf{\Omega}) = \sigma_{\rm el}(\mathbf{\Omega}_0,\mathbf{\Omega}) + \sigma_f \delta(\mathbf{\Omega}_0 - \mathbf{\Omega}), \tag{20}$$

where σ_f is a constant. The physical solution must therefore be insensitive to the transformation of cross section in Eq. (20) although it will indeed change both the elastic mean free path $\lambda_{\rm el}$ and the elastic-collision number distribution $\mathcal{W}_n$ to

$$\tilde{\lambda}_{\mathrm{el}}=\frac{\lambda_{\mathrm{el}}\lambda_f}{\lambda_{\mathrm{el}}+\lambda_f},$$

$$\tilde{\mathcal{W}}_n=\sum_{m=1}^{n}\frac{(n-1)!}{(n-m)!(m-1)!}\frac{\lambda_{\mathrm{el}}^{n-m}\lambda_f^m}{(\lambda_{\mathrm{el}}+\lambda_f)^n}\mathcal{W}_m, \qquad (21)$$

where $\lambda_f=1/(N\sigma_f)$. Equations (21) can be found from the Poisson distribution and are also in agreement with the recurrence relation (1).

However, as could be expected, all quantities whose definition does not directly refer to the number of elastic collisions are invariant with respect to the transformation (20). For example, substituting $\tilde{\lambda}_{\mathrm{el}}$ and $\tilde{\mathcal{W}}_n$ instead of λ_{el} and $\mathcal{W}_n$ into Eq. (4), one finds by simple though cumbersome evaluation that the resulting path-length distribution is equal to the original: $\tilde{\mathcal{Q}}=\mathcal{Q}$. From Eqs. (5) and (7), the same conclusion immediately follows for both $\mathcal{V}_m$ and the energy spectrum. The above argument shows that, in spite of possible ambiguities in forward-elastic scattering and hence in λ_{el} and $\mathcal{W}_n$, the latter may still be used as auxiliary quantities in electron-transport calculations; λ_{el} and $\mathcal{W}_n$ just should be considered as defined *apart from* a transformation such as Eq. (21). However, while, e.g., $\mathcal{Q}$ and $\mathcal{V}_m$ are not sensitive to a renormalization of forward-elastic scattering, convergence of the expansions (4) and (6) may well be, and appropriately selected transformations (21) can be used for improving convergence in some cases.

Note that the invariance of measurable physical quantities with respect to transformations of the cross sections in Eqs. (20) and (21) holds for exact solutions but not for models where only the first few collisions are described accurately while the remaining scattering events are treated within some approximation. One should be aware of this potential problem when using the transport[13] or modified P_1 (Ref. 22) approximation for multiple (>1, 2, or 3) elastic collisions, as well as the model of Oswald, Kasper, and Gaukler.[14,15]

III. NUMERICAL EVALUATION TECHNIQUE AND ITS EFFICIENCY

A. Numerical procedure

For numerical evaluation of W_n, it is convenient to eliminate the singularities ($\sim 1/\eta_0, 1/\eta$) in Eq. (11) by the substitution

$$W_n(\eta_0,\eta)=T_n(\eta_0,\eta)\frac{\eta}{\eta_0+\eta}. \qquad (22)$$

According to Eq. (19), the thus-defined functions T_n are symmetric: $T_n(\eta_0,\eta)=T_n(\eta,\eta_0)$. Recurrence relations for T_n follow immediately from Eq. (11):

$$T_1=K^-, \quad T_n=K^+\times W_{n-1}+W_{n-1}^T\times K^+ + \sum_m W_m^T\times K^-\times W_{n-1-m} \quad \text{for } n\geqslant 2, \qquad (23)$$

where $W_n\equiv W_n(\eta_0,\eta)$, $T_n\equiv T_n(\eta_0,\eta)$, and $K^{\pm}=K^{\pm}(\eta_0,\eta)$, while $W_n^T\equiv W_n(\eta,\eta_0)$; the "product operation" $\times$ is defined by Eq. (12). Neither the functions $T_n(\eta_0,\eta)$ nor any kernels entering Eq. (23) contain singularities in η_0,η; thus Eqs. (23) and (22) are well suited for straightforward numerical tabulation of the elastic-collision number distribution. Note that this calculation scheme (as is generally characteristic for the invariant-embedding approach) does not allow one to limit evaluation of W_n to, e.g., a specific incidence (or emission) angle. Thus, the recurrence relations require $W_n(\eta_0,\eta)$ to be calculated for the whole range $0\leqslant\eta_0,\eta\leqslant 1$ prior to evaluation of W_{n+1} and so the elastic-collision number distribution is necessarily tabulated for *all* incidence and emission angles within a single calculation. Hence, in contrast to Monte Carlo simulations, one does not have the option to reduce computing time by simply reducing the set of considered incidence directions; however, this limitation is compensated by many other advantages.

For a given elastic-scattering cross section, the numerical procedure is naturally split into three steps: (i) First, the kernels $K^{\pm}(\eta_0,\eta)$ are tabulated according to Eq. (13); this is done only once for specific $\mathcal{K}(\eta)$, and the numerical accuracy is chosen to be superior to that of the multiple integrations over direction cosines in part (ii). (ii) $W_n(\eta_0,\eta)$ in the whole range $0\leqslant\eta_0,\eta\leqslant 1$ are sequentially tabulated up to a certain $n=n_m$ in accordance with Eqs. (22) and (23). (iii) Finally, various quantities and dependences of interest are extracted from or calculated with the use of the W_n data saved, including calculations of path-length and inelastic-collision number distributions in accordance with Eqs. (16)–(18). Note that, if the cross-section data utilized has relatively low resolution in scattering angle, a spline fit is made to the data; the resulting $\mathcal{K}(\eta)$, from Eq. (10), will be thought of as exact and perfectly resolved in estimates of the calculation accuracy below.

The integrals involved can be evaluated by a vast variety of simple schemes with comparable merits; we shall only stress nontrivial features and mention those details that are relevant for estimation of computing time and accuracy. The range $[0,1]$ of direction cosines (η_0 and η) is split into N_η grid intervals; the function $W_n(\eta_0,\eta)$ for a given n is thus represented by an array of $(N_\eta+1)^2$ values. The scheme implemented for calculation of $K^{\pm}\times W_m \equiv \int_0^1 K^{\pm}(\eta_0,\eta')W_m(\eta',\eta)d\eta'$ and similar integrals is based upon a three-point polynomial interpolation of W_m; we stress that interpolation of neither $K^{\pm}$ nor the whole integrand is implied. Such a scheme has the advantage that its accuracy is rather insensitive to the behavior of the kernels $K^{\pm}$ (e.g., the sharpness of the forward-scattering peak) because the resulting numerical errors are exclusively due to interpolation of smooth functions W_m, while the relevant coefficients $\sim K^{\pm}$ are once and for all evaluated in part (i) with an accuracy far superior to that obtained from a N_η-point grid.

B. Efficiency of the calculation scheme

Let us now estimate the computing time for the recurrent W_n tabulation [step (ii) above] which is by far the most time-consuming part of the calculation for large n_m and N_η. The basic operation here is evaluation of $K^{\pm}\times W_m$ and similar

integrals that enter Eq. (23). Each integration (for all grid values of η_0, η) takes $\simeq 2N_\eta^3$ floating-point arithmetic operations. The right-hand side of Eq. (23) contains $2(n-1)$ such integrations, so *straightforward* recurrent evaluation of W_n up to $n=n_m$ would require $P(n_m)\simeq 2N_\eta^3 n_m^2$ arithmetic operations. However, there are two simple ways to economize further: (a) Using the symmetry $T_n(\eta_0,\eta)=T_n(\eta,\eta_0)$, one reduces the number of independent terms (to be found by actual integration) in the right-hand side of Eq. (23). (b) Pretabulation of integrals: the integral $W_n^T \times K^-$ is tabulated and saved immediately after W_n has been found, so that, when evaluating all higher-order functions, we perform only one actual integration (instead of two) in each term of the sum in Eq. (23). *Each* of these methods reduces computing time by about a factor of 2, taking our estimate down to

$$P(n_m)\simeq \frac{1}{2}N_\eta^3 n_m^2 . \tag{24}$$

For example, for $N_\eta=100$ and $n_m=100$, the whole calculation for a specific electron energy and target material involves $\simeq 5\times 10^9$ floating-point arithmetic operations. The computing time amounts to $\lesssim 1$ min on a relatively modern PC. This computing speed was judged tolerable; therefore, no further optimization of the scheme was attempted, and most of the calculations presented below were performed with $N_\eta=n_m=100$. The accuracy of the resulting $W_n(\eta_0,\eta)$ is easily tested, e.g., by repeating the calculations with different N_η; as expected, the accuracy depends strongly on N_η and to a much lesser extent on n, η_0, η, and the actual cross section. For $N_\eta=100$ and $n\leqslant 100$, the *relative* errors in the resulting W_n values are typically $\sim 10^{-5}$–10^{-4}. This accuracy usually well exceeds that of typical Monte Carlo simulations and the precision of available cross sections, so for all practical purposes the present scheme's results may be regarded as *exact* for a given cross section. If needed, the calculation time can be appreciably reduced in comparison with the above example. The values $n_m=100$ and $N_\eta=100$ are typically larger than needed for sufficiently accurate REELS- and EPES-related calculations. So while still maintaining an acceptable accuracy, both N_η and n_m may usually be decreased by a factor of 2 or more; the corresponding $P(n_m)$ scales in accordance with Eq. (24) and the computing time may be reduced to seconds on a PC.

Let us now compare the calculation time of the present scheme with that of Monte Carlo simulations. Consider, for example, the simulations depicted in Fig. 2 of Vicanek's paper[6] (W_n for $n\leqslant 50$, carbon target, normal incidence, all emission angles counted). For each value of electron energy, the distributions W_n shown are based on $n_t=10^6$ trajectories. Note that one cannot significantly economize by simple reduction of n_t because moderate irregularities of results are already visible. This is of course due to resolving the number of collisions: e.g., about half of W_n values shown lie below 0.005 and each is therefore contributed to by <5000 trajectories. Now, calculating W_n up to $n=50$, the Monte Carlo program handles *on average* $n_c\sim 25$ collisions per trajectory (this will suffice for an overall estimate, though n_c is seen to depend slowly on E_0: $n_c<25$ for smaller and $n_c>25$ for larger energies depicted). Hence, for each primary energy, Vicanek's Monte Carlo calculation requires

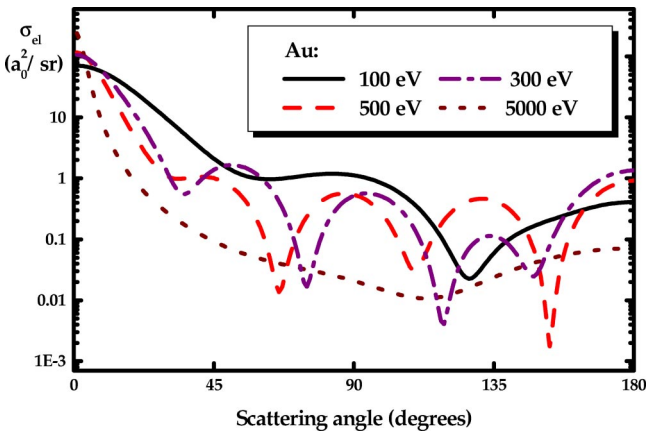

FIG. 2. (Color online) Elastic-collision cross sections σ_{el} (Refs. 20 and 23) for electrons in gold at energies 100, 300, 500, and 5000 eV; units of a_0^2/sr, $a_0\simeq 0.529$Å being the Bohr radius.

$$P_{MC}\simeq n_t n_c P_c \sim 2.5\times 10^7 P_c \tag{25}$$

floating-point arithmetic operations, where P_c is the number of operations required to handle one collision. This is to be compared to Eq. (24): $P(50)\simeq 1.25\times 10^3 N_\eta^3$ for $n_m=50$. Now, P_c entering Eq. (25) may vary somewhat for different Monte Carlo codes, but P_{MC} cannot be much less than, e.g., $P(50)\simeq 1.25\times 10^9$ for $N_\eta=100$ [and must well exceed $P(50)\simeq 1.6\times 10^8$ for $N_\eta=50$]. Thus, in this example, the present scheme (with $n_m=50$, $N_\eta=100$) and the Monte Carlo algorithm are comparable as regards to the needed calculation time. There are, however, drastic differences with respect to the quantities calculated:

(i) While the MC calculation treats a single direction of incidence ($\eta_0=1$ in Ref. 6), the present scheme delivers results for all η_0 at once (with 100-point resolution).

(ii) *Also*, while the MC calculation produces only W_n summed over all emission directions, the present scheme resolves W_n in the angle of emission (again, 100 points).

(iii) *Also*, while the accuracy of the MC results is subject to statistical limitations, the present scheme delivers practically exact results for a given cross section.

All in all, while the MC program resolves *one* variable (the number of elastic collisions n), the present scheme resolves *three* (n, η_0, η) and with better accuracy. Resolving incidence or emission angles or significant improvement of accuracy are of course possible also within the MC scheme, but *any* of these tasks will involve appropriate increase in calculation time, in any case by order(s) of magnitude.

IV. EXAMPLES AND DISCUSSION

In this section we will illustrate some of the capabilities of the formalism presented above. The elastic-scattering cross sections needed for the calculations were taken from the database developed by Jablonski and Tougaard.[20,23] As an ex-

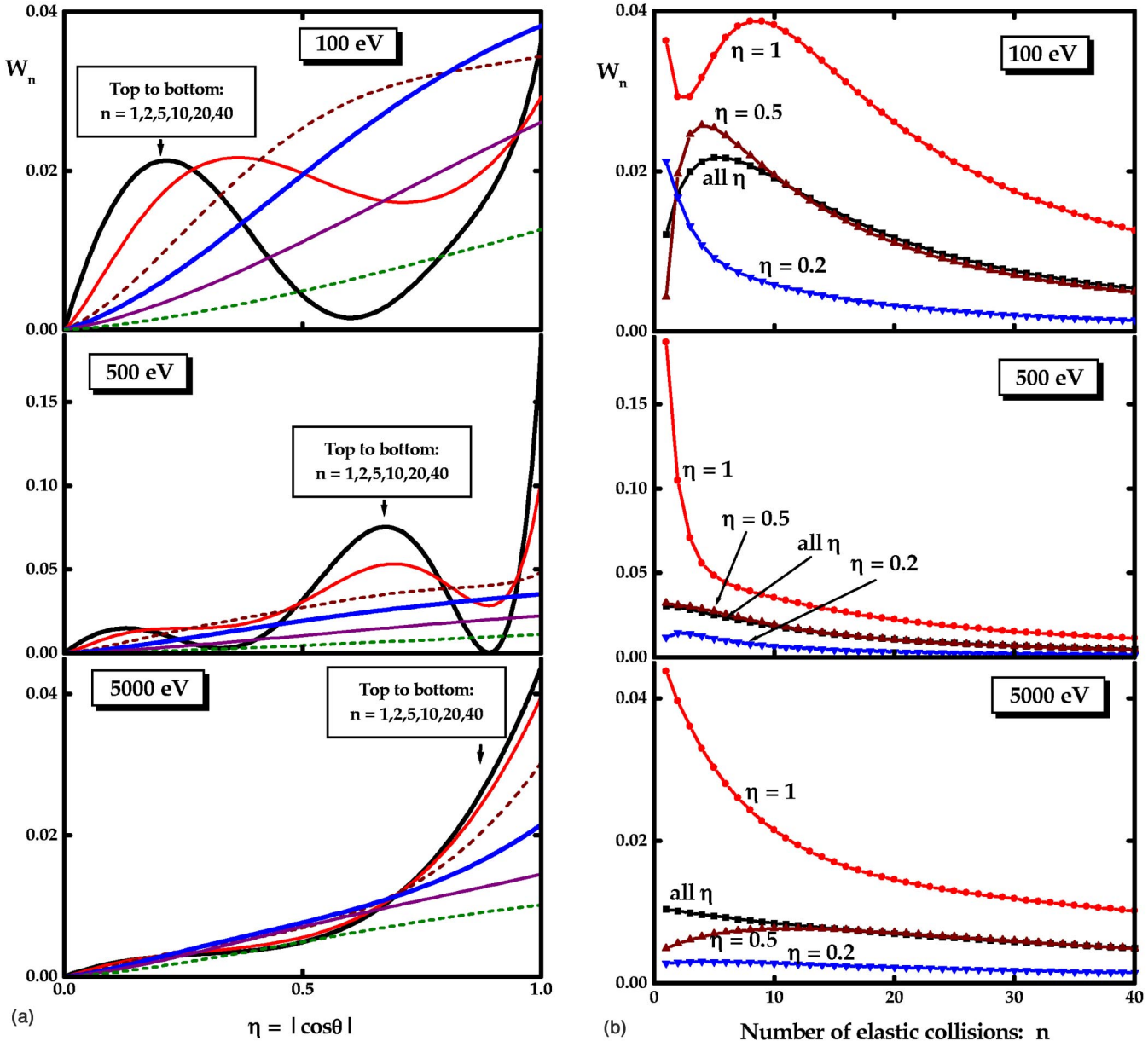

FIG. 3. (Color online) (a) Distributions $W_n(\eta_0=1,\eta)$ in cosine η of emission angle for electrons having experienced a certain number of elastic collisions ($n=1,2,5,10,20,40$). Normal incidence ($\eta_0=1$), Au target, initial energies 100, 500, 5000 eV (top to bottom). (b): Distributions of backscattered electrons in the number of elastic collisions for specific emission angles [$W_n(\eta_0=1,\eta)$ for $\eta=1,0.5,0.2$] indicated on the graphs and summed over all emission directions [$\int_0^1 W_n(\eta_0=1,\eta)d\eta$, marked "all η"]. Normal incidence ($\eta_0=1$), Au target, initial energies 100, 500, 5000 eV (top to bottom).

ample, Fig. 2 shows the cross sections for elastic scattering of 100, 300, 500, and 5000 eV electrons in Au. The results shown in Secs. IV A and IV C are all calculated for gold at these energies, while the examples in Sec. IV D are evaluated for Au and a few other materials.

In all examples depicted below, the direction of the incoming electrons is taken to be normal to the surface ($\eta_0=1$). Note, however, that the calculation scheme described above delivers results for all incidence and emission angles at once; thus, all results shown below for a given energy and target are a minor fraction of those actually obtained within a single program run.

A. Elastic-collision number and path-length distributions

Figure 3(a) shows the elastic-collision number distribution W_n calculated from Eq. (11) for electrons of 100, 500, and 5000 eV energy in gold as a function of $\eta=|\cos\theta|$ ($\eta=1$ corresponds to electron emission normal to the surface and $\eta\simeq 0$ to glancing electron emission). For glancing emission angles with $\theta-90°<15°$ ($\eta<0.25$), it is seen that $W_1>W_n$ for all $n\geqslant 2$ although there is also a significant contribution from electrons that have undergone more than one scattering event. For larger emission angles, the multiply scattered electrons contribute more and, e.g., at 100 eV and $\eta=0.5$ both W_1 and W_2 are smaller than W_n for all n

$=3$–10; as evident from Fig. 3(b), the same property holds also for the elastic-collision number distribution summed over all emission directions.

The distributions W_1 of electrons emitted after a single elastic collision demonstrate significant variation of their shapes with energy. In accordance with Eqs. (13) and (15), W_1 for normal incidence is simply related to the elastic-collision cross section for scattering angles $>90°$: $W_1(\eta_0=1,\eta)=2\pi\mathcal{K}(-\eta)\,\eta/(1+\eta)$. Thus, apart from the factor $2\pi\eta/(1+\eta)$ common for all targets and energies, the distributions W_1 reflect the behavior of the respective cross sections and therefore vary with energy as much as the curves shown in Fig. 2 (at scattering angles $>90°$). Due to integrations in Eq. (11), the distributions W_n for larger n are generally smoother and less sensitive to the details of the underlying cross sections. Apart from normalization, the shapes of the high-order distributions become similar for different energies: with increasing n, W_n are seen to gradually approach the $\sim\eta$ dependence corresponding to an isotropic flux of emitted electrons, but even for the largest n depicted in Fig. 3(a), W_n still deviate appreciably from the simple $\sim\eta$ law.

Figure 3(b) shows corresponding distributions W_n in the number n of elastic collisions for various emission angles as well as those integrated over all emission directions. For $n\leqslant 5$, W_n may increase or decrease with increasing n depending on the energy and angle of emission. Except for near-normal emission ($\eta=1$), the general trend is that W_n decreases rather slowly with n and the fraction of emitted electrons in a given direction that have undergone a few and, e.g., 40 elastic scattering events is comparable. Because of this result, models that expand the spectrum in terms of multiple elastic-scattering events need a large number of terms. This is due to the high cross section for small-angle elastic scattering (see Fig. 2).

Figure 3(b) demonstrates that the elastic-collision number distribution W_n may either monotonically decrease with n or have a maximum at $n>1$. For distributions integrated over emission direction, the issue was analyzed in some detail in Ref. 6. In the numerical examples therein (cf. Figs. 2 and 3 in Ref. 6), all distributions W_n for a carbon target have a maximum at $n>1$ while those for gold decrease monotonically; this distinction could be readily attributed to the differences of scattering cross sections for heavier and lighter atoms. Figure 3(b) covers a wider range of electron energies and thus illustrates a wider range of options, indicating, e.g., that the angle-integrated distribution for gold also becomes nonmonotonic for sufficiently low energy. Resolving the direction of emission adds another dimension to the issue as — even for fixed energy and target — the shape of the distribution is seen to drastically depend on η. For example, for 100 eV electrons, Fig. 3 shows a wide range of possible distributions: monotonic decrease for $\eta=0.2$, a maximum at $n=4$ for $\eta=0.5$, and even a distribution with two peaks (at $n=1$ and $n=8$) for $\eta=1$.

Figure 4 shows the corresponding distributions of path lengths for the emitted electrons calculated from Eq. (16) and given in units of λ_{el}^{-1}; the respective values of λ_{el} (as determined from the cross sections plotted in Fig. 2) are

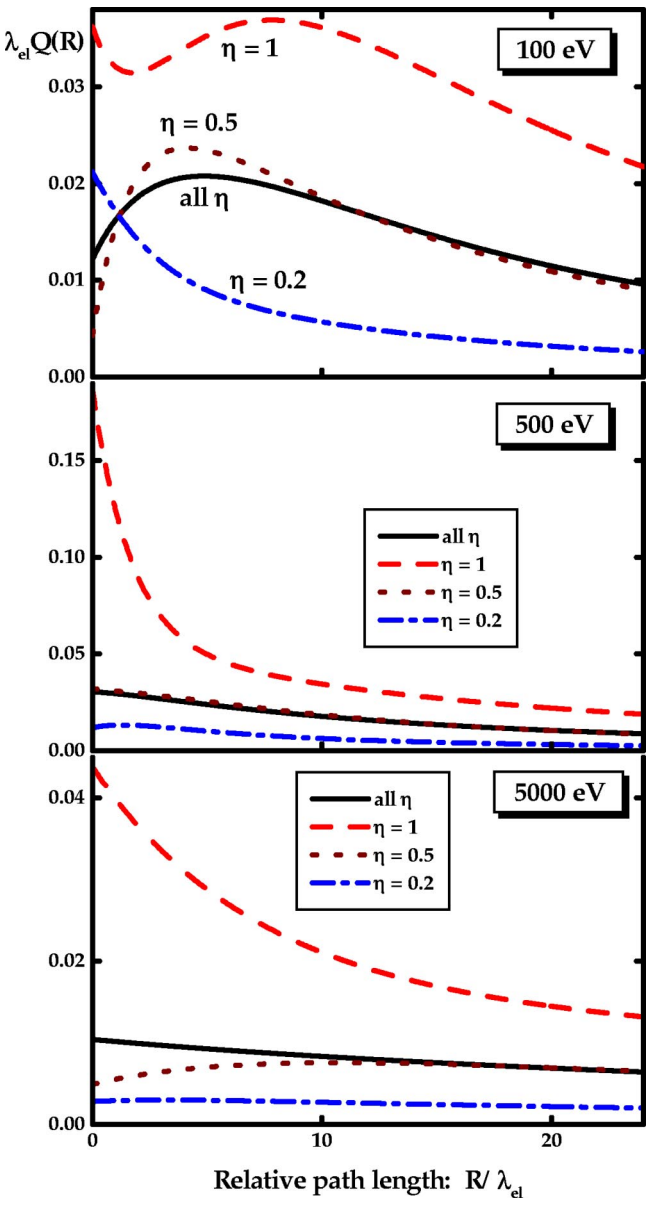

FIG. 4. (Color online) Distributions $Q(\eta_0,\eta;R)$ of emitted electrons in path length traveled within the solid calculated from Eq. (16) and given in units of λ_{el}^{-1}. The distributions are for specific emission angles ($\eta=1,0.5,0.2$ as indicated on the graphs) and summed over all emission directions (marked "all η"). Normal incidence ($\eta_0=1$), Au target, initial energies 100, 500, 5000 eV (top to bottom); the respective values of λ_{el} (as determined from σ_{el} in Fig. 2) are $\lambda_{el}=1.70,3.91,11.82$ Å .

listed in the caption to Fig. 4. Due to statistical correlation between path length and the number of elastic collisions, the depicted path-length distributions closely reproduce the shapes of the respective W_n in Fig. 3(b), although the transition from $W_n(\eta_0,\eta)$ versus n to $Q(\eta_0,\eta;R)$ versus R/λ_{el} results in a smoothening effect.[6] In particular, the path-length distributions in Fig. 4 show the same variety of shapes and peak locations as discussed above for W_n; in general, this situation discourages the use of simple and inflexible models for $Q(\eta_0,\eta;R)$.

B. Extraction of the inelastic mean free path

From Eqs. (17) and (18), the elastic-peak intensity is

$$V_0(\eta_0,\eta)=\sum_{n=1}^{\infty}\left(\frac{\lambda_{in}}{\lambda_{el}+\lambda_{in}}\right)^n W_n(\eta_0,\eta). \qquad (26)$$

Since W_n are non-negative, Eq. (26) is a monotonic function of $\lambda_{in}/(\lambda_{el}+\lambda_{in})$. Therefore Eq. (26) allows one to uniquely extract λ_{in} if W_n and λ_{el} are known and the elastic-peak intensity is measured for a given angle of emission. This is the basic idea behind the EPES method.[8–11]

To test the procedure, the values of inelastic mean free path used in this paper were determined in this way from the Monte Carlo results of Dubus *et al.*[15] for the elastic-peak intensities which thus served as a substitute for experimental V_0 data. Extracted λ_{in} values were in particular used for evaluation of the elastic-peak intensity, from Eq. (26); cf. Sec. IV D for comparison with original Monte Carlo data[15] for a range of solids and energies. Elastic-collision cross sections utilized in Ref. 15 were the same as in the present calculations, and the λ_{in} extraction procedure accurately reproduced the IMFP values according to the general TPP-2M formula[24] underlying the MC calculations. In particular, the resulting inelastic-collision number distributions and elastic-peak intensities (cf. Secs. IV C and IV D) were practically identical to those obtained by direct application of the TPP-2M formula for λ_{in}; minor deviations were observed only in a few cases associated with significant inaccuracies of the MC results; cf. Sec. IV D below.

As expected, in most cases the λ_{in}-extraction procedure provided equivalent results when applied for different ranges of emission angles. There were a few exceptions, however, most notably Cu and Au at 300 eV and Ag at 500 eV [cf. Figs. 8(b)–8(d) below]; as discussed in Sec. IV D, in these cases the Monte Carlo results are appreciably inaccurate, and caution had to be exercised when picking the range of emission angles for extraction of λ_{in}. To the extent that other factors (such as, e.g., surface excitations and surface roughness) can be neglected, this example shows that the requirement of the extracted IMFP being independent of the emission and incidence angles can be easily utilized to test whether the elastic-collision cross section used and calculation procedure applied are consistent with measured elastic-peak intensities.

C. Inelastic collision-number distribution

Figure 5 shows the distributions V_{0n} of electrons emitted without inelastic scattering according to the number n of elastic-scattering events for various emission angles. In accordance with Eq. (18), for fixed incidence and emission angles, V_{0n} is simply related to W_n: $V_{0n}(\eta_0,\eta)=W_n(\eta_0,\eta)/(1+\lambda_{el}/\lambda_{in})^n$; i.e., V_{0n}/W_n monotonically decreases with increasing n. Thus, compared to the total elastic-collision number distribution, large-n contributions to *elastic-peak intensity* are strongly reduced due to statistical correlation between the numbers of elastic and inelastic collisions suffered by an electron. In particular, compared to W_n, V_{0n} is more likely to decrease monotonically which is confirmed by comparison of Figs. 3(b) and 5. However, the decrease still is not fast enough to neglect the higher-order V_{0n} contributions altogether: for example, except for angles of emission close to the surface plane, Fig. 5 indicates a significant contribution to the elastic peak from electrons that have been elastically scattered more than 5 times.

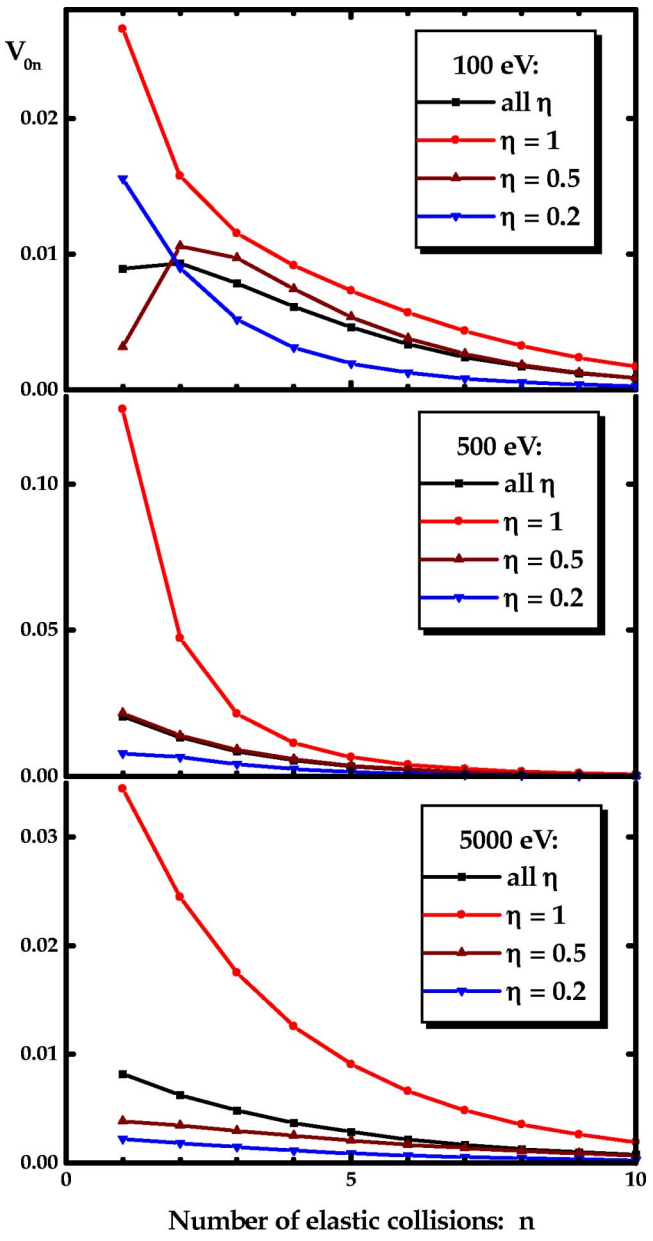

FIG. 5. (Color online) Distributions $V_{0n}(\eta_0=1,\eta)$ of *elastically* backscattered electrons according to the number of elastic collisions, n. Plotted are distributions for a few specific emission angles ($\eta=1,0.5,0.2$) and all emission directions [$\int_0^1 V_{0n}(\eta_0=1,\eta)d\eta$, marked "all η"]. Normal incidence ($\eta_0=1$), Au target, initial energies 100, 500, 5000 eV (top to bottom).

Figures 6(a) and 6(b) show the distributions V_{0n} and V_{1n}, respectively, as a function of $\eta=|\cos\theta|$. V_{0n} is the angular distribution of electrons emitted without inelastic scattering and V_{1n} the distribution of electrons that have been inelastically scattered once. It is clearly seen that, as expected, the

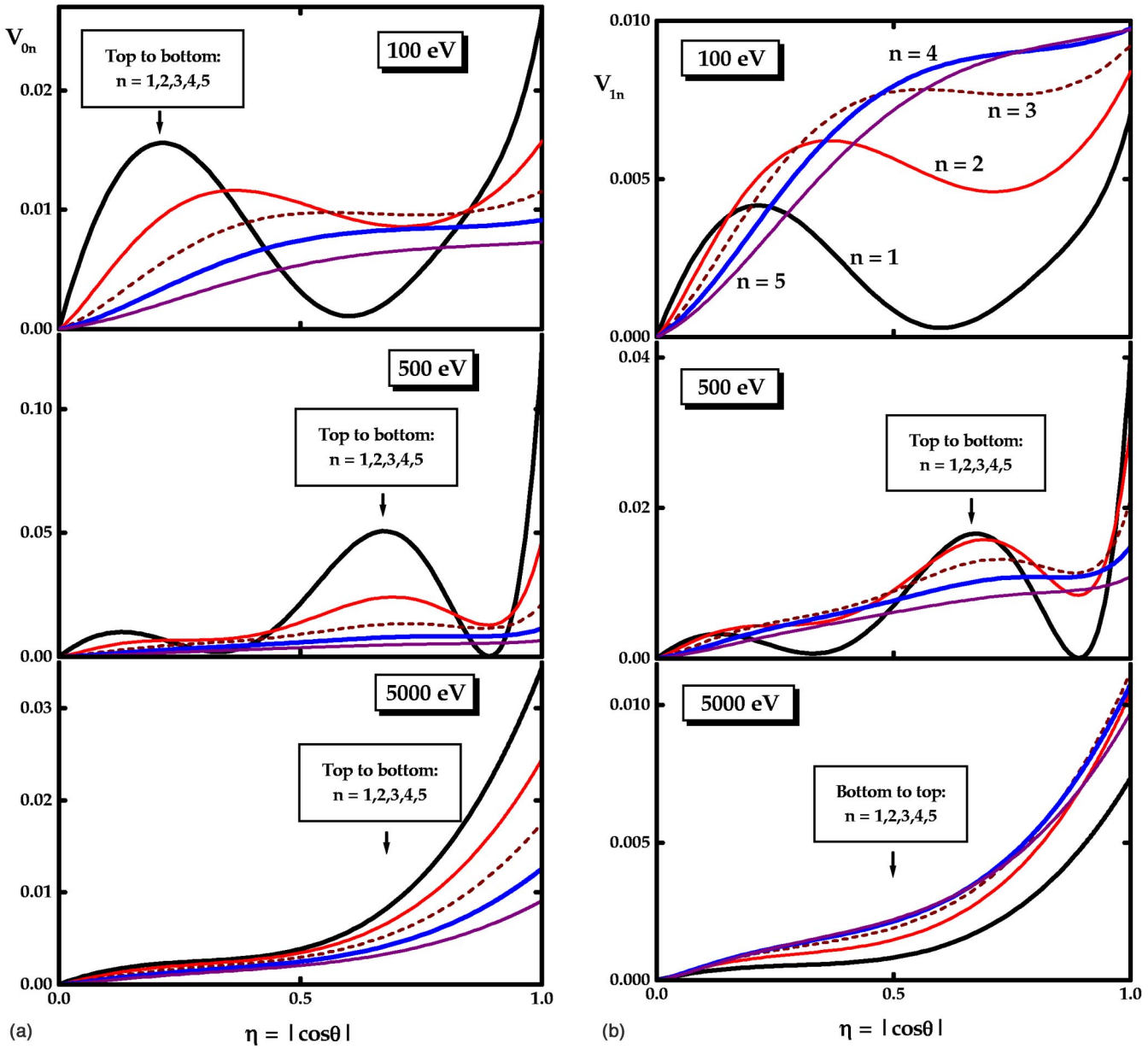

FIG. 6. (Color online) (a): Distributions $V_{0n}(\eta_0=1,\eta)$ in cosine η of emission angle for electrons *elastically* backscattered after a certain number ($n=1,\ldots,5$) of elastic collisions. Normal incidence ($\eta_0=1$), Au target, initial energies 100, 500, 5000 eV (top to bottom). (b): Distributions $V_{1n}(\eta_0=1,\eta)$ in cosine η of emission angle for electrons backscattered after a *single inelastic* and a certain number ($n=1,\ldots,5$) of elastic collisions. Normal incidence ($\eta_0=1$), Au target, initial energies 100, 500, 5000 eV (top to bottom).

relative importance of electrons that experienced multiple elastic collisions is larger for V_{1n} than for V_{0n}.

The distribution V_m of electrons that have undergone m inelastic collisions (regardless of the number of elastic-scattering events) has been calculated from Eq. (17) and is shown in Figs. 7(a) (distributions in emission direction for various m) and 7(b) (distributions in the number of inelastic collisions for various angles of emission). Note that, due to correlation between the path length and the number of inelastic collisions, the distributions in Fig. 7(b) are still smoother but otherwise very similar to the path-length distributions in Fig. 4.

The above results indicate that significant inaccuracies may be expected from models in which the first two scattering events are treated exactly while a rough approximation is used to describe multiply scattered electrons. The use of such models is especially problematic when the energy loss spectrum is calculated because then the relative contributions from large path lengths (and thereby from W_n for large n) are more important. Note, however, that even for evaluation of the elastic-peak intensity, both the transport and the OKG approximation have been found to give significant deviations from Monte Carlo simulations.[15,25]

It should be noted that the present approach regards rel-

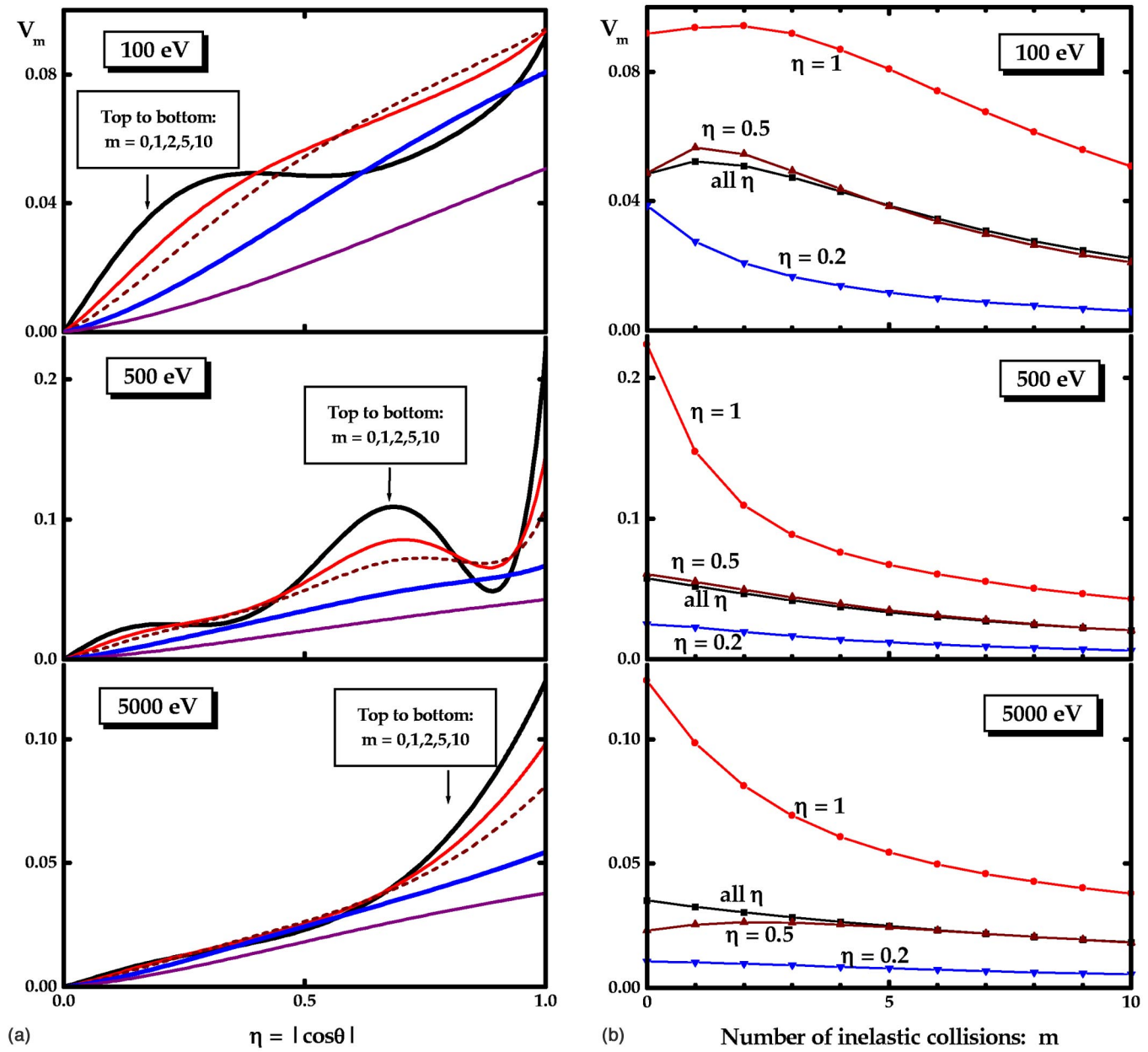

FIG. 7. (Color online) (a) Distributions $V_m(\eta_0=1,\eta)$ in cosine η of emission angle for electrons having experienced a certain number of inelastic collisions ($m=0,1,2,5,10$). Normal incidence ($\eta_0=1$), Au target, initial energies 100, 500, 5000 eV (top to bottom). (b): Distributions of backscattered electrons in the number of inelastic collisions for specific emission angles [$V_m(\eta_0=1,\eta)$ for $\eta=1,0.5,0.2$] indicated on the graphs and summed over all emission directions [$\int_0^1 V_m(\eta_0=1,\eta)d\eta$, marked "all η"]. Normal incidence ($\eta_0=1$), Au target, initial energies 100, 500, 5000 eV (top to bottom).

evant cross sections as functions of the initial energy of the incident electrons but independent of further energy changes. This is no problem for the calculation of the elastic peak. This approximation is also feasible for calculations of various distributions as long as the relative energy loss is small but it may limit the validity of results corresponding to electrons that have undergone a significant relative energy loss. This is most problematic at low energies. The typical energy loss in a single inelastic scattering event is $\sim 5-20$ eV.[18] Therefore, e.g., the results for 100 eV electrons in Fig. 7 may be inaccurate for $n \gtrsim 2-3$. Similarly $Q(R)$ in Fig. 4 at 100 eV is expected to be inaccurate for $R/\lambda_{in} \gtrsim 2-3$, though still may be used, e.g., for the calculation of V_0 and V_1 from Eq. (5).

D. Elastic peak: Comparison with Monte Carlo results

Over the past decade, several approximations for the calculation of the angular distribution of elastically backscattered electrons have been proposed. In a recent critical review,[15] the accuracy and range of validity of various analytical models were investigated. In that paper, a Monte Carlo simulation was taken as the exact reference and the

validity of the individual models was judged by the deviation from this reference.

In this section we show that the present solutions give an excellent comparison to the Monte Carlo calculations and that in those cases where deviations occur these are actually due to deficiencies of the Monte Carlo scheme. The elastic-peak intensity distribution is $V_0(\eta_0,\eta)$. However, to get reasonable statistics, the probabilities of elastic backscattering in Ref. 15 were summed over emission-angle intervals of 4.5°. To compare to $V_0(\eta_0,\eta)$, the resolution of the present calculations must be artificially lowered. We have therefore plotted

$$\int_{\cos 4.5°\,n}^{\cos 4.5°(n-1)} V_0(\eta_0,\eta)\,d\eta = \int_{180°-4.5°\,n}^{180°-4.5°(n-1)} V_0(\eta_0,|\cos\theta|)\sin\theta\;d\theta \quad \text{versus} \quad 4.5°(2n-1)/2,$$

as well as the continuous distribution $(\pi/40)V_0(\eta_0,|\cos\theta|)\sin\theta$ where the normalization factor $(\pi/40)\text{rad}=4.5°$.

The results for Al, Cu, Ag, and Au at various energies are shown in Figs. 8 (a)–8(d). Except for a few cases, the agreement with the Monte Carlo simulations is excellent. The exceptions are Cu at 300 eV, Ag at 500 eV, and Au at 300 eV. The reason for the discrepancy lies in the limitations of the Monte Carlo scheme: the applied random number generator for the elastic-scattering events does not sample the angles correctly when the cross section shows several maxima and minima as a function of the scattering angle. This problem was acknowledged in the review paper[15] and is further illustrated here for Au at 100 and 300 eV in Fig. 9 where the probabilities of elastic backscattering after one ($\sim V_{01}$), two ($\sim V_{02}$), and $\geqslant 3$ ($\sim \Sigma_{n\geqslant 3} V_{0n}$) elastic collisions are compared to the Monte Carlo results.[15] For 100 eV, the agreement is good, while for 300 eV there are large deviations. The latter deviations are seen to originate primarily from the $n=1$ contribution (described by an *exact* formula within the present approach; cf. Secs. II B and IV A) which is most sensitive to the shape of the elastic-collision cross section at scattering angles $>90°$: for normal incidence considered here, the $n=1$ contributions in Fig. 9 (left) are

$$\sim W_1(\eta_0=1,\eta)\sin\theta \sim \mathcal{K}(-|\cos\theta|)\frac{\sin\theta|\cos\theta|}{1+|\cos\theta|}. \qquad (27)$$

Comparing the calculated distributions to the underlying elastic-collision cross sections (like, e.g., those in Fig. 2), one concludes that the random number generator used in Ref. 15 is inappropriate when there are sharp extrema of σ_{el} in scattering angle; such features are associated with the most drastic deviations between the present and Monte Carlo results. For example, the cross section for Au at 300 eV (cf. Fig. 2) exhibits two sharp minima at scattering angles $>90°$, which are seen to result in the pronounced minima at $180° - \theta \sim 30°$ and 60° of the $n=1$ and total 300 eV distributions in Figs. 8(d) and 9 (left), which, however, are smeared out in respective Monte Carlo results. Likewise, the two minima of the 500 eV cross section in Fig. 2 — at scattering angles $\simeq 153°$ and 110° — result in the minima of the 500 eV angle distribution in Fig. 8(d) at $180° - \theta \simeq 25°$ and 73°, respectively; the 2°–3° deviations between locations of the distribution's minima in Fig. 8(d) and those of the underlying cross section are due to the angle-dependent factor (additional to $\mathcal{K}$) in Eq. (27) and the $n>1$ contributions to the distribution. The minima of the resulting 500 eV distribution in Fig. 8(d) are not as pronounced as those for 300 eV and do not differ as much from the respective Monte Carlo results; however, as expected, the largest relative deviations ($\simeq 15\%$) are observed at $180° - \theta \simeq 25°$, i.e., in the vicinity of the minimum associated with the sharpest extremum of the elastic-collision cross section in Fig. 2.

V. SUMMARY AND OUTLOOK

We have studied an application of the invariant-embedding approach for evaluation of the probability distributions of electrons backscattered from a solid surface. The basic formalism was developed by Vicanek[6] who gave an important contribution to the fundamental understanding of REELS but resorted to Monte Carlo simulations in order to obtain explicit solutions. In the present paper, we demonstrated that deterministic invariant-embedding equations are more effectively solved numerically. It has been shown above that the resulting calculation scheme demonstrates significant advantages over the Monte Carlo approach as regards to both accuracy and CPU time required.

However, along with its advantages, our approach presently has significant limitations. As is usually characteristic of analytical treatments, the assumptions implied above make the present scheme less generally applicable than, e.g., Monte Carlo simulations. Although the simplifications used are typically suitable (and are in fact rather common) for REELS- and EPES-related calculations, the present scheme may not be applicable in a more general context, e.g., for a comprehensive description of electron backscattering. Let us list here the most important limitations implied above.

(i) The scheme is limited to the case of sufficiently small *relative* energy loss. This gives rise to a number of simplifications: variation of cross sections with instantaneous electron energy is neglected; angular and energy loss scattering events are statistically uncoupled and ascribed to, respectively, elastic and inelastic collisions; secondary electrons are disregarded.

(ii) The target is assumed to be semi-infinite and homogeneous, with an ideal planar surface. Thus, the technique cannot be directly utilized for analysis of concentration profiles of inhomogeneous samples, etc.

(iii) While some applications in REELS to scattering as a function of azimuth angle would be highly desirable, in this paper only azimuth-integrated quantities were considered. Consequently, the graphical examples refered exclusively to the case of normally incident electrons, although in fact the

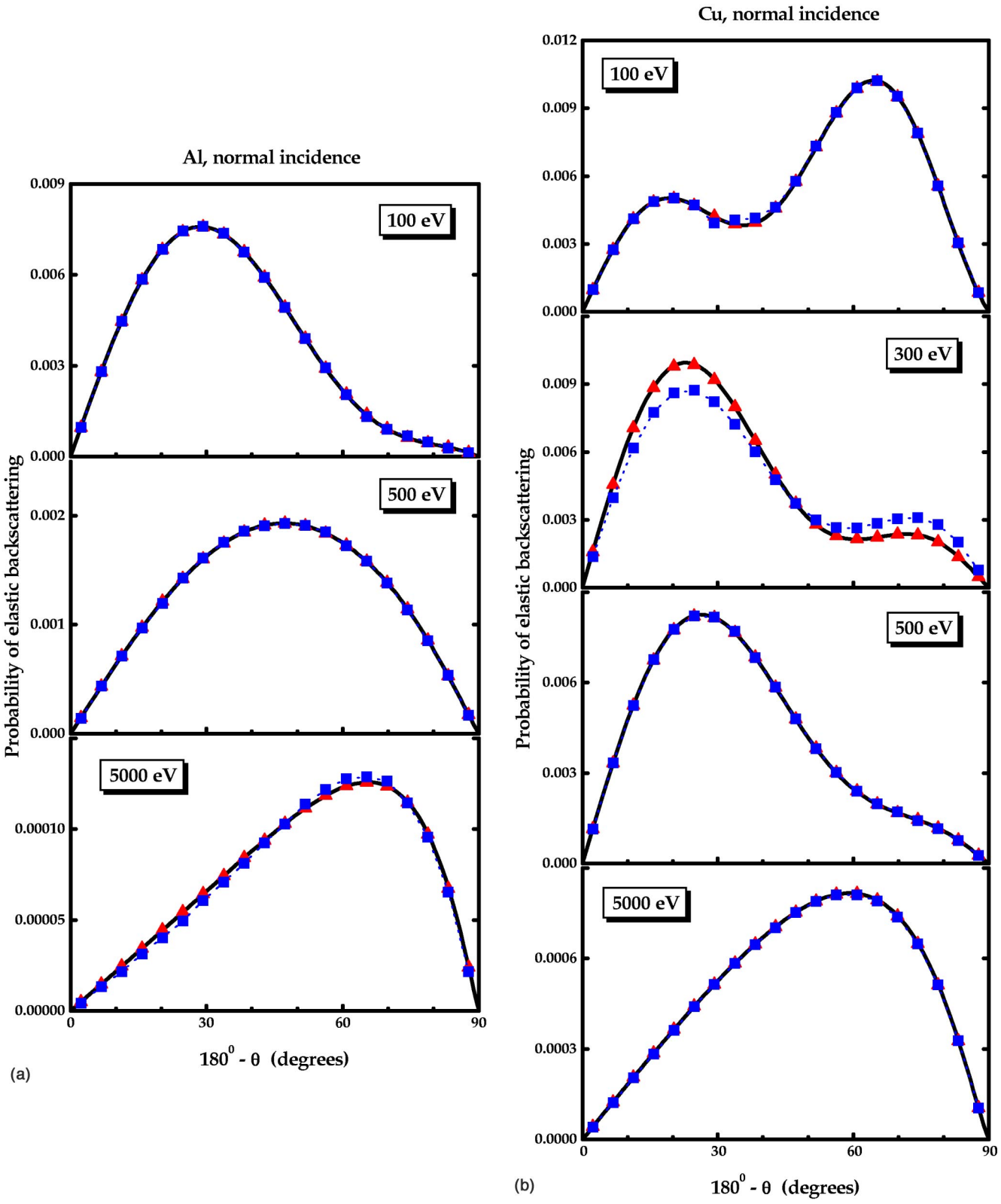

FIG. 8. (Color online) (a) Probability of elastic backscattering within emission-angle intervals $180° - \theta = [4.5°(n-1) - 4.5°n]$. Triangles: present results. Squares: Monte Carlo results of Ref. 15. Solid lines show continuous distributions $(\pi/40)V_0(\eta_0 = 1, |\cos\theta|)\sin\theta$ in emission angle (present calculations). Normal incidence ($\eta_0 = 1$), Al target, electron energies 100, 500, 5000 eV (top to bottom). (b) Same as (a) for Cu target and energies 100, 300, 500, 5000 eV. (c) Same as (a) for Ag target. (d) Same as (a) for Au target and energies 100, 300, 500, 5000 eV.

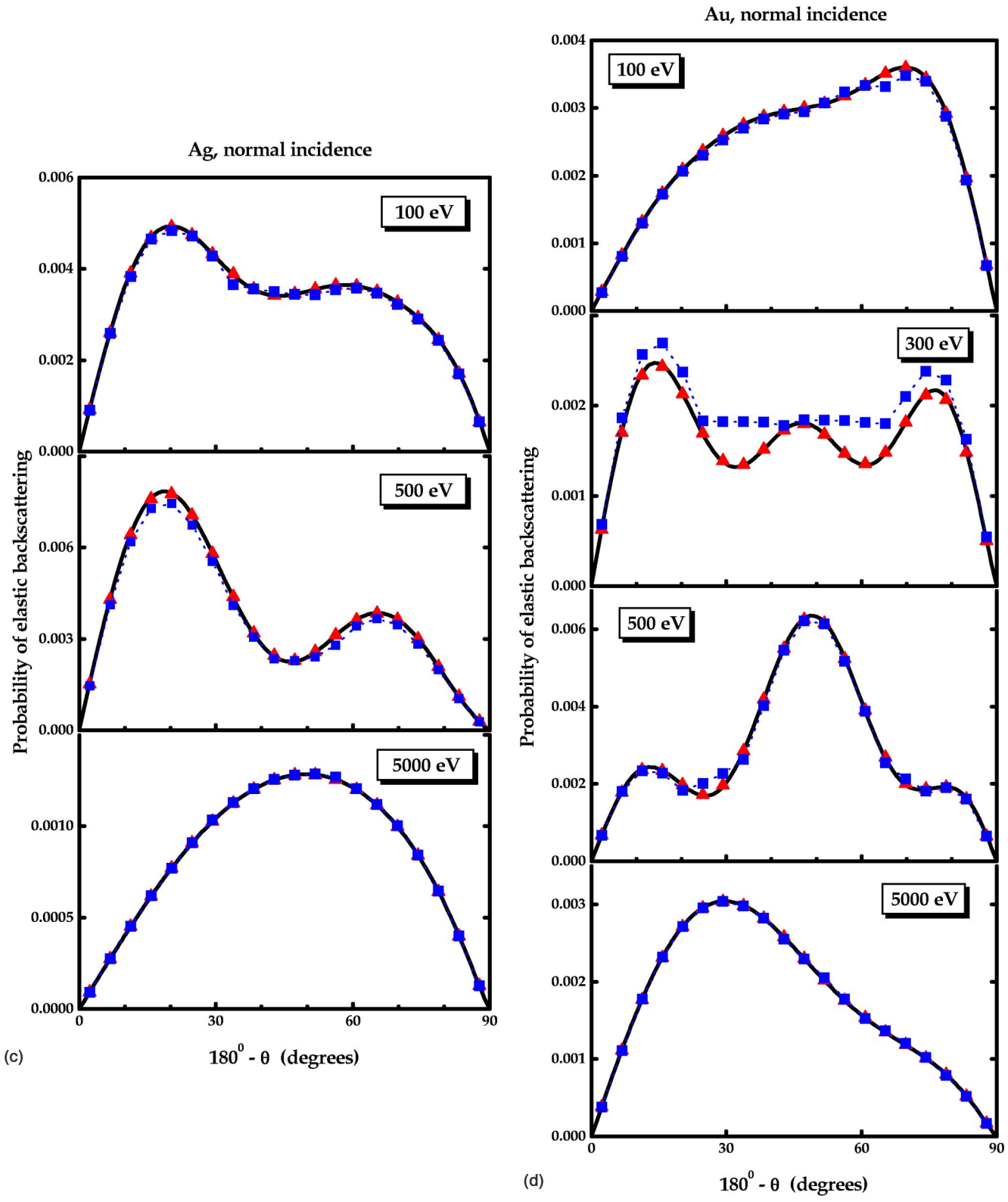

FIG. 8. (*Continued*).

applied calculation scheme produces simultaneously similar results for all incidence angles.

The latter limitation here is relatively easy to overcome. It turns out that the present scheme is readily generalized to include computations with fully resolved azimuths, *additionally* to the variables treated above. It is really striking that — in contrast to other approaches including Monte Carlo — additional resolving of azimuths within the present formalism is performed *without* appreciable loss of accuracy or significant increase of CPU time; the latter typically in-

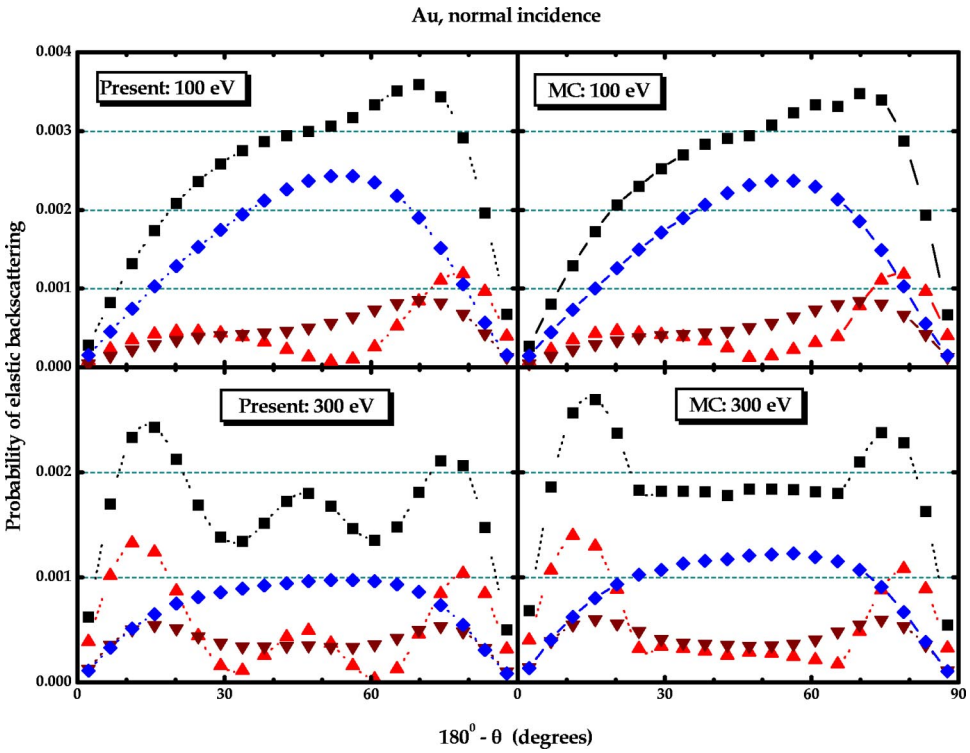

FIG. 9. (Color online) Comparison of present (left) and Monte Carlo (Ref. 15) (right) results for the total elastic-backscattering probability [as in Fig. 8(d)] and partial contributions corresponding to certain numbers $n(1,2,\text{or}\geqslant 3)$ of elastic collisions. Total current: squares. $n=1$: up triangles. $n=2$: down triangles. $n\geqslant 3$: diamonds. Normal incidence ($\eta_0=1$), Au target, electron energy 100 eV (top) and 300 eV (bottom).

creases only by a factor of 2 or less compared to the azimuth-integrated calculations described above. Such an extension of the calculation scheme and azimuth-resolved results will be presented in a forthcoming paper.

The first two items above are not as trivial. While the equations of Sec. II are readily generalized to include arbitrarily large energy losses and/or inhomogeneous targets, straightforward extension of the numerical scheme to those cases would be associated with a drastic or even prohibitive increase of the computing effort required and/or likewise decrease of accuracy. A more appealing technique may be based upon a nontrivial modification of the invariant-embedding approach; such a work is now in progress.

ACKNOWLEDGMENTS

Illuminating discussions with M. Vicanek and P. Sigmund are gratefully acknowledged. This work has been supported by the Danish Natural Science Research Council (SNF) and EU Contract No. ERBIC15-CT960800.

*Corresponding author. FAX: (+45) 6615 8760. Electronic address: svt@fysik.sdu.dk.

[1] H. Raether, *Surface Plasmons on Smooth and Rough Surfaces and on Gratings*, Springer Tracts in Modern Physics, Vol. 111 (Springer, New York, 1980).
[2] S. Tougaard and I. Chorkendorff, Phys. Rev. B **35**, 6570 (1987).
[3] S. Tougaard, Surf. Interface Anal. **11**, 453 (1988).
[4] S. Tougaard, Surf. Sci. **464**, 233 (2000).
[5] S. Tougaard and J. Kraaer, Phys. Rev. B **43**, 1651 (1991).
[6] M. Vicanek, Surf. Sci. **440**, 1 (1999).
[7] W. S. M. Werner, Surf. Interface Anal. **31**, 141 (2001).
[8] A. Jablonski, Surf. Sci. **151**, 166 (1985).
[9] A. Jablonski, B. Lesiak, and G. Gergely, Phys. Scr. **39**, 363 (1989).
[10] C. J. Powell and A. Jablonski, J. Phys. Chem. Ref. Data **28**, 19 (1999).
[11] V. S. M. Werner, C. Tomastik, T. Cabela, G. Richter, and H. Stori, Surf. Sci. **470**, 123 (2001).
[12] V. M. Dwyer, Surf. Interface Anal. **20**, 513 (1993).
[13] V. S. M. Werner, I. S. Tilinin, and M. Hayek, Phys. Rev. B **50**, 4819 (1994).
[14] R. Oswald, E. Kasper, and K. H. Gaukler, J. Electron Spectrosc. Relat. Phenom. **61**, 251 (1993).
[15] A. Dubus, A. Jablonski, and S. Tougaard, Prog. Surf. Sci. **63**, 135 (2000).
[16] S. Chandrasekhar, *Radiative Transfer* (Oxford University Press, New York, 1950).
[17] R. F. Dashen, Phys. Rev. A **134**, A1025 (1964).
[18] S. Tougaard, Surf. Interface Anal. **25**, 137 (1997).
[19] W. S. M. Werner, Surf. Interface Anal. **23**, 737 (1995).
[20] A. Jablonski and S. Tougaard, Surf. Interface Anal. **22**, 129 (1994).
[21] V. M. Dwyer and J. M. Richards, Surf. Interface Anal. **18**, 555 (1992).
[22] Y. F. Chen, C. M. Kwei, and P. Su, J. Phys. D **28**, 2163 (1995).
[23] A. Jablonski and S. Tougaard, *NIST Elastic-Electron-Scattering Cross-Section Database* version 1.0 user's guide (U.S. Department of Commerce, Technology Administration, National Institute of Standards and Technology Standard Reference Data Program, Gaithersburg, MD, 1996).
[24] S. Tanuma, C. J. Powell, and D. R. Penn, Surf. Interface Anal. **21**, 165 (1994).
[25] A. Jablonski, Surf. Interface Anal. **29**, 582 (2000).